IEEE Access
Multidisciplinary ⋮ Rapid Review ⋮ Open Access Journal

Received 7 March 2024, accepted 22 April 2024, date of publication 29 April 2024, date of current version 7 May 2024.

Digital Object Identifier 10.1109/ACCESS.2024.3394506

RESEARCH ARTICLE

DC-Bus Capacitor Discharge Method Based on Bleeder and Windings for Electric Vehicles in Emergency

XIAOJUN ZHANG AND JIAQIANG YANG, (Senior Member, IEEE)
College of Electrical Engineering, Zhejiang University, Hangzhou 310027, China

Corresponding author: Jiaqiang Yang (yjq1998@163.com)

This work was supported by the Aeronautical Science Foundation of China under Grant 20230028076008.

ABSTRACT The bleeding circuit is important for dropping the dc-bus voltage to safe voltage when electric vehicles (EVs) encounter an emergency. However, the bleeding circuit may be bulky and heavy to ensure that the total discharge operation can be completed in the specified time (5 seconds). In order to reduce the volume and weight of the bleeding circuit, this paper proposes a maximum discharge power method that can maintain the discharge power of the bleeding resistor and windings at the maximum discharge power. The mechanism and disadvantage of traditional uncontrolled rectification (UR) method is analyzed for illustrating the necessity of reducing the bleeding resistor at first. Then, the proposed maximum discharge power is developed based on the established power flow model. For the sake of improving the tracking performance and dynamic performance of the discharge power, an adaptive sliding mode power control (ASMPC) is proposed with the adaptive reaching law, which can effectively reduce the chatting effect on inner current loop. Finally, the proposed strategy is validated on a permanent magnet synchronous motor drive used for EVs, and the results show that the proposed discharge method can not only reduce the bleeding resistor size and weight but also improve the dynamic characteristics.

INDEX TERMS Bleeding resistor, dc-bus capacitor, maximum discharge power, permanent magnet synchronous machine (PMSM), power flow model.

I. INTRODUCTION

Due to the advantages of environmental friendliness, high efficiency and low cost, electric vehicles (EVs) have attracted considerable attention [1], [2], [3], [4], [5]. Permanent magnet synchronous machine (PMSM) shows superiorities in EVs with high power density, high efficiency and compact structure [6], [7], [8]. Typically, the high voltage drive systems of EVs include PMSMs, three-phase inverter, film capacitor, high voltage breaker, bleeder circuit and lithium battery. Although high voltage can extend the driving distance and reduce losses, it also brings about higher requirements for the safety of EVs, especially in emergency [9], [10].

When an emergency happens to the EVs, e.g., car crash, the propulsion system will enter in protection mode that the breaker mode that the breaker will be tripped and the inverter will be shut off. Simultaneously, the PMSMs shaft is disconnected from the gearbox, and the motor rotates without load. However, the back electromotive force of the PMSM and the dc-bus capacitor will keep the dc-bus voltage at the high voltage, which will cause electric shock risks to passengers and rescuers. In order to protect passengers from electric shock in the event of collisions, United Nation Vehicle Regulation ECCE R94 requires that the dc-bus voltage should drop to the safe voltage (60V) within 5s [11]. Due to the electric vehicle in emergency condition at this time is short and special, it does not belong to the traditional electric vehicle drive cycle condition, so the drive cycle method cannot be used to analyze this process.

In order to achieve the goal of 5-s discharge, many discharge methods have been proposed, which can be divided

The associate editor coordinating the review of this manuscript and approving it for publication was Kan Liu.

into two categories: motor winding-based method [12], [13], [14], [15], [16], and bleeding resistor-based method [17], [18], [19]. For the motor winding-based method, the motor windings are used as the bleeding resistor, and the energy is dissipated in the form of heat. In [12], a large d-axis current and zero q-axis current is injected into the PMSM. The zero q-axis current can reduce the conversion of kinetic energy to electrical energy in the discharge process. Thus, the motor back EMF can be rapidly reduced to zero by flux-weakening. Nevertheless, this method may have overcurrent issues as the rotor speed is higher. In order to solve this problem, [13] and [14] proposed a three-stage constant voltage discharge strategy. At the first stage, the bus voltage is rapidly reduced to the safe voltage under the effect of the field-weakening. Then, the proportional integral (PI) controllers control the dc-bus voltage at the safe voltage until the speed decreases to safe speed. Finally, the d-q axis current gradually becomes zero. Although the three-stage discharge method can quickly reduce the dc-bus voltage to a safe level, this method is no longer effective when the first stage fails to reduce the bus voltage to the safe voltage. Reference [15] presented a q-axis current segmented discharge method when the PMSM drive system with large inertia and small safe current. The segmented q-axis current is obtained by making the power consumption of the windings copper smaller than the electromagnetic power of the regenerative braking. However, winding-based discharge methods is sensitive to system parameters, such as system inertia, machine speed and system safe current. Therefore, it has very few industrial applications.

Another commonly-used discharge method is the bleeding resistor-based method that is composed of a power switch and a bleeding resistor. The power switch is turned on when the system receives a discharge request, as well as the kinetic energy of the motor and the electrical energy stored in the capacitor is dissipated through the bleeding circuit. As the inverter works in an uncontrolled rectification state during the discharge, this method is also called the uncontrolled rectification (UR) discharge method. In [16], a resistive brake is designed to dissipate the excess energy when the motor decelerates. On the basis of the above bleeding circuit-based discharge topology, [17] adds optocouplers and Zener diodes to the discharge circuit. This method not only realizes the isolation of the control circuit and the power circuit through the optocoupler, but also realizes good protection for the bleeder circuit. In order to make the bleeding circuit more energy-saving and easy to maintain, [18] proposes a bleeding circuit with high space utilization method. Through designing the dc-bus capacitor discharge drive circuit, the system can detect the dc-bus voltage changes and the stage of the controller pin, so as to avoid the mis-discharge when the bus voltage is not disconnected, and to improve the reliability of the discharge. Nevertheless, the above-mentioned bleeding resistor-based method do not fully utilize the discharge capacity of the bleeding resistor. Besides, the bleeding resistor is not only bulky and heavy but also has low discharge power density.

By keeping the discharge power of the bleeding resistor to the maximum can speed up the discharge process and reduce the size and weight of the bleeding resistor. However, it is difficult to achieve maximum power control only by conventional PI controllers, which has long setting time and overshoot. Therefore, a power outer loop controller with strong robust and high dynamic performance is required. It is well known that the sliding mode control (SMC) has the advantages of excellent dynamic performance and strong robustness. In [19], for the boost converter for fuel cell systems, an active disturbance rejection control (ADRC) combined with the SMC for the sake of improving the robustness of the system. In [20], to deal with the problem of insufficient torque tracking, a novel SMC strategy was proposed, which greatly improved the system robustness and dynamic response speed. However, the SMC can cause chattering problems when the system state quantity reaches the sliding mode surface. In order to reduce the chattering of sliding surface, [21], [22] estimated and compensated the system disturbance and parameter perturbation, thereby reducing the gain of the SMC and reducing the system chattering. Another way to reduce the gain is to improve the reaching law, such as [23] introduce a new sliding-mode reaching law that composed of system state variable and the power term of sliding surface function to suppress the chattering and reduce the time of reaching to the sliding mode surface. In [24], a new adaptive terminal sliding mode reaching law is proposed, it can be seen as an improvement on the exponential reaching law. Typically, the conventional sliding mode power control (CSMPC) will bring chattering due to the inherent characteristics. Hence, the chattering should be reduced, especially when the CSMPC is used as an outer loop controller.

To reduce the size and weight of the bleeding resistor, this article proposes a maximum discharge power method that can keep the discharge power at maximum power. In addition, the adaptive sliding mode power control (ASMPC) is proposed with adaptive reaching law for improving the discharge power tracking performance and reducing the chatting. The main novelties of this paper are listed as follows:

1) The traditional UR discharge method model is established for analyzing and calculating the bleeding resistor size and weight, illustrating that the traditional UR discharge method needs to be improved.

2) The maximum discharge power strategy is proposed based on the established power flow model, which can not only keep the maximum discharge power of the bleeding resistor, but also maintain the motor windings at the maximum discharge power. Compared with the traditional UR discharge method, the size and weight of the designed bleeding resistor is reduced significantly.

3) For improving the discharge power tracking performance, the ASMPC based on adaptive reaching law is

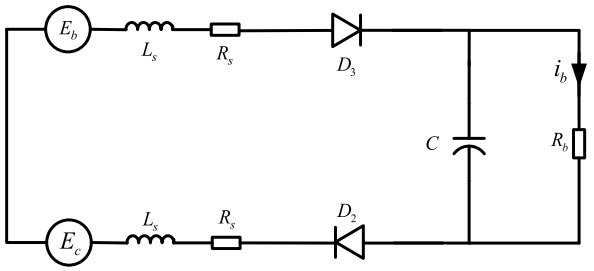

FIGURE 1. The schematic diagram of traditional UR discharge method.

proposed. As the ASMPC adopts an adaptive reaching law that can adapt to variations in the sliding surface and system states, the chatting is reduced greatly.

The rest of this article is organized as follows. The traditional UR discharge model is established and analyzed in Section II. Section III introduces the proposed maximum discharge power method and designs the bleeding resistor based on proposed method. In Section IV, the proposed ASMPC with the adaptive reaching law is presented. The experimental results are presented in Section V. Finally, Section VI concludes this article.

II. MECHANISM AND DISADVANTAGE OF TRADITIONAL UR DISCHARGE METHOD

In this section, the mechanism and disadvantage of the traditional UR discharge method is analyzed based on the established model. Then, the size and the weight of the bleeding resistor are discussed according to the system parameters, illustrating that the conventional discharge method is need to be improved for reducing the volume and weight.

A. MODEL OF TRADITIONAL UR DISCHARGE METHOD

Assuming that the core saturation, eddy current loss and hysteresis loss is ignored and harmonics and saturation is not considered, the mathematical model of PMSM in the rotating d-q frame are given by [25], [26], and [27].

$$\begin{cases} u_{\mathrm{d}} = R_{\mathrm{s}} i_{\mathrm{d}} + L_s \dfrac{di_{\mathrm{d}}}{dt} - \omega_e L_{\mathrm{s}} i_{\mathrm{q}} \\ u_{\mathrm{q}} = R_{\mathrm{s}} i_{\mathrm{q}} + L_s \dfrac{di_{\mathrm{q}}}{dt} + \omega_e L_{\mathrm{s}} i_{\mathrm{d}} + \omega_e \psi_m \\ T_e = \dfrac{3}{2} p \psi_{\mathrm{m}} i_q \\ J \dfrac{d\omega_m}{dt} = T_e - B\omega_m - T_L \end{cases} \tag{1}$$

where u_d, u_q and i_d, i_q are the stator voltage and current, respectively. L_s is the stator inductance; R_s is the stator resistance, ψ_m is the rotor flux and ω_e, ω_m the electrical angular speed and mechanical angular speed, respectively. p is the pole pair number, J, B and T_{L} are inertia, mechanical damping coefficient and mechanical load torque, respectively.

If the EVs encounter an emergency, the inverter will be shut off and the PMSM works as a generator. More importantly, the six free-wheeling diodes constitute uncontrolled rectifier, the schematic diagram of bleeding resistor discharge is shown in Fig.1.

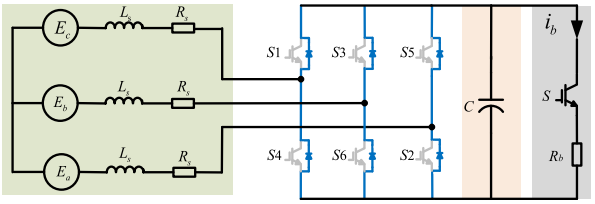

FIGURE 2. Simplified electrical circuit model of uncontrolled rectification.

The generator back electromotive force (EMF) can be expressed as

$$\begin{cases} E_a = E_0 \sin(\omega_e t) \\ E_b = E_0 \sin(\omega_e t - 2\pi/3) \\ E_c = E_0 \sin(\omega_e t + 2\pi/3) \end{cases} \tag{2}$$

The back EMF amplitude E_0 can be expressed as

$$E_0 = \omega_e \psi_m \tag{3}$$

During the discharge process, only the uncontrollable rectifier bridge composed of diodes works. Therefore, one diode on each of the upper and lower bridge arms is turned on at the same time, and the turn-on voltage is the largest of the motor line voltages, which can be expressed as

$$E_{out} = \max\{E_{ab}, E_{ac}, E_{bc}, E_{ba}, E_{ca}, E_{cb}\} \tag{4}$$

In order to analyze the relationship between the dc-bus voltage and the current, assuming the $E_{out} = E_{bc}$. As the E_{bc} is greater than other line voltages, diodes D_3 and D_2 are turn on, and the circuit model can be simplified as Fig.2.

According to Kirchhoff's voltage law:

$$E_b - E_c = 2i_b R_s + 2L_s \frac{di_b}{dt} + 2V_{on} + i_b R_b \tag{5}$$

where the V_{on} is the turn on voltage of the diode. Substitute (2) into the above equation, the result is

$$2i_b R_s + 2L_s \frac{di_b}{dt} + 2V_{on} + i_b R_b = \sqrt{3}\omega_e \psi_m \sin(\omega_e t - \frac{\pi}{6}) \tag{6}$$

Considering that the dc-bus has a big capacitor, the bus voltage at steady state can be expressed as

$$u_{dc} = i_b R_b = \sqrt{3}\omega_e \psi_m - 2i_b R_s - 2V_{on} \tag{7}$$

Therefore, the real-time discharge current is

$$i_b = \frac{\sqrt{3}\omega_e \psi_m - 2V_{on}}{R_b + 2R_s} \tag{8}$$

During the discharge of the bus capacitors, the current of the bleeding resistor provides braking torque. In order to reduce the analytical complexity, the speed of machine can be considered as a linear decrease [28]. Therefore, the average discharge current can be approximated as

$$i_{b\_ave} \approx \frac{\sqrt{3}\left(\omega_{e0} + \omega_{th}\right)\psi_m - 4V_{on}}{2\left(R_b + 2R_s\right)} \tag{9}$$

TABLE 1. Main parameters of the prototype.

Parameters	Value	Parameters	Value
Stator resistance	0.3Ω	Pole number	4
PM flux linkage	0.125Wb	Moment of inertia	0.3kg·m^2
Rated speed	209rad/s	Maximum current	30A
d-axis inductance	1.1mH	DC-bus voltage	310V
q-axis inductance	1.1mH	DC-bus capacitor	420uF

where ω_{th} is the threshold speed at which the line-to-line back EMF is equal to safe voltage, ω_{e0} is the initial electrical angular velocity.

The total expended energy can be expressed as

$$Q_{dis} = \frac{J}{2}\left(\omega_{m0}^2 - \omega_{th}^2\right) + \frac{1}{2}C\left(U_0^2 - U_{safe}^2\right) \tag{10}$$

where ω_{m0} is the initial mechanical rotating speed, U_0 is the initial dc-bus voltage that is equal to battery voltage.

For the sake of reducing the bleeding resistor size and weight, the discharge time can be set to 5s when the motor is running at rated speed. Hence, with the discharge time, resistance of the bleeding resistor can be derived as

$$R_b = \frac{5\left(\sqrt{3}\left(\omega_{e0} + \omega_{eth}\right)\psi_m - 4V_{on}\right)^2}{2\left\{J\left(\omega_{m0}^2 - \omega_{mth}^2\right) + C\left(U_0^2 - U_{safe}^2\right)\right\}} - 2R_s \tag{11}$$

B. DESIGN AND ANALYSIS OF THE BLEEDING RESISTOR

Generally, the material of the wire wound power resistor is the alloy of nickel (Ni) and chromium (Cr) [29]. In order to evaluate the size and weight of the bleeding resistor, nickel-chromium 80 is used as the resistance material in this paper. The resistivity and density of the Nichrome wire are $1.08 \cdot 10^{-6}\Omega \cdot$ m and 8310 kg/m^3, respectively. Since the current- carrying capacity of the wire is affected by the diameter, the relationship between the wire diameter and the current-carrying capacity is obtained by quadratic fitting, which is shown in Fig.4.

$$i_{cap} = 0.6582d^2 + 3.138d - 0.04954 \tag{12}$$

According to the average discharge current, the properties of the bleeding resistor are shown in Table 2 with system parameters in Table 1.

From the table 2, it can be found that the bleeder resistance is 11.7 Ω, the diameter of the nichrome wire is 2.3 mm and the length is 30.1 m, weighing around 1.04 kg. However, the huge bleeding resistor will not only increase vehicle weight but also reduce the practicality of the bleeding resistor-based method. Therefore, the discharge method for dc-bus capacitor with small and light bleeding resistors is urgently needed for EVs.

TABLE 2. The parameters of bleeding resister.

Parameters	value
resistance (Ω)	11.7
Diameter (mm)	2.3
average current (A)	10.9
wire length (m)	30.1
resistor weight (kg)	1.04
resistor size (m^3)	1.25×10^{-4}

III. PROPOSED MAXIMUM DISCHARGE POWER METHOD

Since the bus voltage decreases with the decline of the speed, the discharge power of the bleeding resistor decreases gradually. For the purpose of improving discharge density of the bleeding resistor, it is significant to maximize the discharge power during the discharge process.

A. POWER FLOW MODEL DURING THE DISCHARGE PROCESS

Based on the schematic diagram of traditional UR discharge method in Fig.1, the dc-bus capacitor current can be expressed as.

$$C\frac{du_{dc}}{dt} = i_{dc} - \frac{u_{dc}}{R_b} \tag{13}$$

According to the power balance on both sides of the power converter, it can be derived that

$$u_{dc}i_{dc} = -\frac{3}{2}\left(u_d i_d + u_q i_q\right) \tag{14}$$

Substituting (1) and (13) into (14) yields

$$\frac{C}{2}\frac{du_{dc}^2}{dt} + \frac{u_{dc}^2}{R_b} = -\frac{3}{2}\left(R_s i_d^2 + R_s i_q^2 + L_d i_d\frac{di_d}{dt} + L_q i_q\frac{di_q}{dt} + \omega_e\psi_{\mathrm{m}} i_q\right) \tag{15}$$

The power equation under steady state can be expressed as

$$\frac{C}{2}\frac{du_{dc}^2}{dt} + \frac{u_{dc}^2}{R_b} = -\frac{3}{2}\left(R_s\left(i_d^2 + i_q^2\right) + \omega_e\psi_m i_q\right) \tag{16}$$

In order to increase the copper consumption of the system, the dq-axis current should be always on the current limit circle, hence

$$\underbrace{\frac{C}{2}\frac{du_{dc}^2}{dt}}_{P_c} = \underbrace{-\frac{3}{2}\omega_e\psi_m i_q}_{P_e} \underbrace{-\frac{3}{2}R_s I_{\max}^2}_{P_{cu}} \underbrace{-\frac{u_{dc}^2}{R_b}}_{P_b} \tag{17}$$

where P_{c}, P_{e}, P_{cu} and P_{b} are dc-bus capacitor power, electromagnetic power, copper loss power and bleeding resistor power, respectively. As it can be seen in (17), a part of

the electromagnetic power is converted into the copper loss of the machine windings and the power of the external bleeder, the remaining part is converted into the dc-bus capacitor power. Therefore, increasing the discharge power of the bleeding resistor can speed up the discharge process. However, the discharge power of the bleeding resistor usually is limited for cost and size. It is necessary to keep the maximum discharge power of the bleeding resistor in order to save space and cost.

B. DESIGN OF BLEEDING RESISTOR

During the maximum discharge power process, the energy dissipated by the machine windings can be derived as

$$Q_{wind} = \frac{3}{2} R_s I_{\max}^2 t_d \tag{18}$$

Since the flux-weakening current is injected into d-axis, the threshold speed ω_{th2} is lower than ω_{th}.The total discharge energy can be expressed as

$$C\frac{du_{dc}}{dt} = i_{dc} - \frac{u_{dc}}{R_b} \tag{19}$$

Then, the power consumed by the bleeding resistor is

$$P_{ex} = \frac{Q_{dis2} - Q_{wind}}{t_d} \tag{20}$$

In order to prevent surges in the bus voltage, we let the maximum dc-bus voltage satisfy

$$U_{\max} \le \sqrt{3}\omega_{e0}\psi_m - 2V_{on} \tag{21}$$

Considering that the bleeding resistor is a purely resistive load, the power can also be expressed as

$$P_{ex} = u_{dc} i_{cap} \tag{22}$$

As the discharge power is constant, the discharge voltage should take the maximum value for the sake of reducing the wire diameter and thus wire mass.

Hence, the resistance of the bleeding resistor can be derived as

$$R_b = \frac{\left(\sqrt{3}\omega_{e0}\psi_m - 2V_{on}\right)^2}{P_{ex}} \tag{23}$$

Based on the parameters of the PMSM drive system, the parameters of the designed bleeding resistor are shown in Table 3. Compared with Table 2, although the designed bleeder resistance increases to 36.8 Ω, the wire diameters drop to 1.3mm.

Table 4 shows the specific comparative results of the traditional UR discharge method and the proposed maximum discharge power method. Compared with the traditional UR discharge method, the weight of the bleeding resistor reduced from 1.04 to 0.50kg (52%) and the size drops to $6.0 \times 10^{-5}\text{m}^3$(52%). More importantly, it is visible that the discharge power density of the proposed method is higher than the traditional UR discharge method. The reason why the power density of the proposed method is higher than that of the traditional UR discharge method is that the discharge power of the traditional method gradually decreases as the machine speed goes down, while proposed the method can keep the discharge power of bleeding resistor and machine windings at the maximum value. Consequently, the proposed discharge method can reduce the bleeder volume and size.

TABLE 3. The parameters of bleeding resister based on proposed method.

Parameters	value
resistance (Ω)	36.8
diameter (mm)	1.3
average current (A)	4.9
wire length (m)	45.2
resistor weight (kg)	0.50
resistor size (m^3)	6.0×10^{-5}

IV. DESIGN OF ASMPC BASED MAXIMUM DISCHARGE POWER

In order to design the power controller for the bleeding resistor, the power flow model is established. Then, the CSMPC is applied to account for improving the dynamic performance. Considering that the output of the CSMPC is the input of the current inner loop, the chattering of the CSMPC will cause the q-axis current to ripple. Therefore, this article proposes an adaptive reaching law to reduce the chattering.

A. MAXIMUM DISCHARGE POWER BASED ON CSMPC

It is obviously that (17) is nonlinear equation, which can be solved by applied local linearization-based PI strategy. However, it has the disadvantage of sensitivity to operation point shift when the speed decreases. Therefore, in order to linearize the dynamic (17), define $P_b = u_{dc}^2/R_b$, then (17) is transformed as

$$\frac{dP_b}{dt} + \frac{2P_b}{CR_b} = -\frac{3}{CR_b}\left(R_s I_{\max}^2 + \omega_e \psi_m i_q\right) \tag{24}$$

Consider the disturbance exists in the system during the discharge process, (24) can be rewritten as

$$\frac{dP_b}{dt} = -\frac{2P_b}{CR_b} - \frac{3R_s I_{\max}^2}{CR_b} - \frac{3\omega_e \psi_{\text{m}} i_q}{CR_b} + d(t) \tag{25}$$

where $d(t)$ is the total disturbance.

The tracking error of discharge power is expressed as

$$e = P_b^* - P_b \tag{26}$$

where P_b^* is the reference power of the bleeding resistor. The derivative of e can be obtained as

$$\dot{e} = \frac{2P_b}{CR_b} + \frac{3R_s I_{\max}^2}{CR_b} + \frac{3\omega_e \psi_{\text{m}} i_q}{CR_b} - d(t) \tag{27}$$

TABLE 4. The comparison of dc-bus capacitor discharge method.

Type of method	Bleeding resistor quality(kg)	Bleeding resistor size（m^3）	Discharge power density(W/kg)
Traditional UR	1.04	1.25×10^{-4}	1160
Proposed method	0.5	6.0×10^{-5}	1767

The integral sliding surface is shown as follows

$$s = e + c\int_0^t edt \tag{28}$$

where c>0 is the positive gain. The conventional exponential reaching law is selected for the sake of improving the dynamic quality of the approach motion, which is expressed as

$$\dot{s} = -ks - \varepsilon sgn\,(s)\ ,\ \ k > 0,\ \varepsilon > 0 \tag{29}$$

According (26) to (29), the reference q-axis current can be obtained as

$$i_q^* = \frac{(-ks - \varepsilon sgn(s) - ce)\,R_bC - 2P_b - 3R_sI_{\max}^2}{3\omega_e\psi_m} \tag{30}$$

From (27), it can be known that the reaching speed is related to the choices of ε and k. Although increasing ε and k can improve the reaching speed, it also increases the chattering. Therefore, the gain of the reaching law requires careful consideration of the approach time and chattering.

B. ASMPC BASED ON AN ADAPTIVE REACHING LAW

To further suppress the influence of CSMPC chattering on the inner current loop, an adaptive reaching law is proposed to decrease the chattering and reaching time, which is expressed as

$$\dot{s} = f(e,s) = -k\,|e|^{\alpha}\,s - \varepsilon\frac{\left(1+\lambda-e^{-\delta|s|}\right)}{\lambda+e^{-\delta|s|}}\,|e|^{\beta}\,sgn\,(s) \tag{31}$$

where k>0, λ >0, ε >0, 0< α <1, β >1, δ is a constant.

It can be seen that the adaptive reaching law consists of variable isokinetic approach term and variable exponential reaching term. The amplitude of symbolic function can be adjusted by the proposed reaching law with adapting the state variable e to control the convergence rate. When the system initial state is far away from the sliding surface (|e| and |s| increase), isokinetic approach term and exponential reaching term work simultaneously. Thus, *f(e,s)* will converge to $-k\,|e|^{\alpha}\,s - \varepsilon(1+\lambda)\,|e|^{\beta}/\lambda$, which is much larger than the traditional gain of the exponential reaching law. While the system state approaches the sliding mode surface (|e| and |s| increase), *f(e,s)* will converge to $-\lambda\varepsilon\,|e|^{\beta}/(\lambda+1)$, in which system state |e| gradually decrease to 0. Therefore, the adaptive sliding reaching law can not only reduce the reaching time, but also reduce the chattering on the sliding mode surface. More importantly, by introducing the system state into the sliding mode reaching law, the reaching speed is further accelerated and the chattering is reduced.

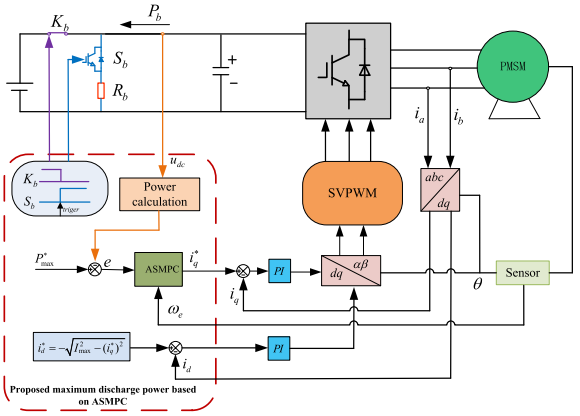

FIGURE 3. Block diagram of the proposed discharge method.

Substitute (27) and (28) into (31), the reference *q*-axis current can be rewritten as

$$i_q^* = \frac{(f\ (e,s) - ce)\,R_bC - 2P_b - 3R_sI_{\max}^2}{3\omega_e\psi_m} \tag{32}$$

In order to verify the stability of the proposed ASMPC with adaptive reaching law, a candidate Lyapunov function is expressed as

$$V = \frac{s^2}{2} \tag{33}$$

Based on (31), the derivation of (33) can be derived as

$$\dot{V} = s\cdot\dot{s} = -k\,|e|^{\alpha}\,s^2 - \varepsilon\frac{\left(1+\lambda-e^{-\delta|s|}\right)}{\lambda+e^{-\delta|s|}}\,|e|^{\beta}\,|s| \le 0 \tag{34}$$

Evidently, the proposed ASMPC satisfies the stability requirement, and the actual discharge power will track the given discharge power.

To take the full advantage of discharge capacitor, the machine wingdings discharge power should also be maximum. Hence, the *d*-axis current should be set as

$$i_d^* = -\sqrt{I_{\max}^2 - (i_q^*)^2} \tag{35}$$

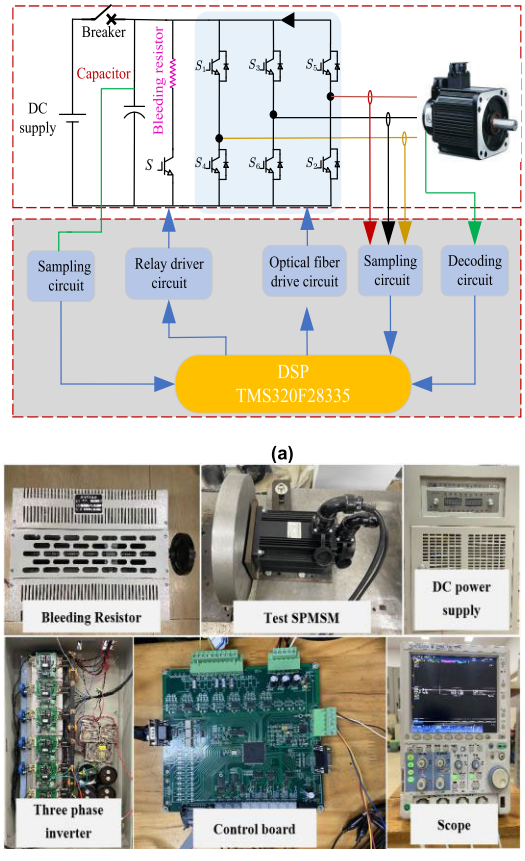

FIGURE 4. Test platform. (a) Circuit diagram. (b) Experimental setup.

The block diagram of the proposed discharge strategy is shown in Fig. 3. As shown, the outer power loop applies ASMPC with the adaptive reaching law.

V. EXPERIMENTAL VERIFICATION

A. PREPARATION FOR THE EXPERIMENT

To verify the proposed maximum discharge power of bleeding resistor based on ASMPC, experiments are conducted on a three-phase SPMSM whose parameters are listed in Table 1. The experimental circuit diagram and experimental setup are depicted in Fig. 4(a) and (b), respectively.

The overall system is mainly composed by a 3.8kW SPMSM, bleeding resistor, three phase inverter and DC power supply. The value of bleeding resistor can be regulated by adjusting the wire-wound sliding varistor. In the experiment, the resistance of the bleeding resistor is 36.8 Ω. A dc power supply is set to 310 V. A three-phase insulated gate bipolar transistor inverter is used as the voltage source inverter (VSI) with the frequency of 10 kHz. The thin-film capacitor, U13-424NT 420μF, is connected in parallel with the VSI. The breaker, EV200A, is connected in series on the dc-bus between the dc power supply and the thin-film capacitor. In order to simulate the real inertia of EVs motor, the SPMSM is coaxially connected to an inertia flywheel.

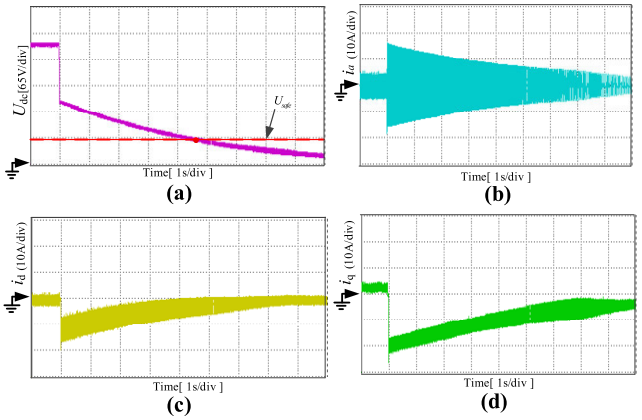

FIGURE 5. Experimental results of the maximum discharge power based on the proposed ASMPC at the speed of 1000 r/min. (a) DC-bus voltage; (b) d-axis current; (c) Discharge power of the external bleeder; (d) q-axis current.

The DSP TMS320F28335 is used to validate the proposed discharge method.

B. EXPERIMENTAL RESULTS

Fig. 5 demonstrates the experimental results when the discharge request arises at the speed of 2000r/min under the UR discharge method. Fig.5(a) shows that it takes nearly 4.5s for the bus voltage to decrease to the safe voltage with the designed bleeding resistor. As the discharge method without special designed current, the phase current decreased with the machine speed declined in Fig.5(b). Consequently, the discharge power descended, which lead to a heavy weight of the discharge resistor. Fig.5(c) and Fig.5(d) present the d-axis current is much smaller than the q-axis current, because most of the kinetic energy of the motor was converted into resistance thermal energy.

Fig. 6 shows the experimental results of maximum discharge power based on PI, CSMPC and the ASMPC when the discharge request occurs at 1 s under the speed of 2000r/min. As it can be seen from Fig.6(a), the dc-bus voltage drops to safe voltage within 4.5s with three different controllers, being a little shorter than 5 s. This happens because the mechanical friction and inverter losses are ignored when building the model. In addition, the response time of PI, CSMPC and ASMPC are 0.3s, 0.12s, and 0.08s, respectively, which proves that the proposed ASMPC has the fastest response time. Furthermore, the bus voltage overshot of PI control method is 65V, which is larger than 25V that of the CSMPC method. In contrast, the proposed ASMPC method has almost no overshoot in the voltage. As for the discharge power in Fig.6(b), when the reference discharge power jumps to the maximum power, the PI control method causes an overshoot of 300W. However, the proposed ASMPC strategy only experiences an overshot of 110W, which is smaller than 210W that of the CSMPC method. More importantly, the discharge power ripple of PI control method is evidently large, while the ripples in the CSMPC case are reduced a little but still larger than that in the proposed ASMPC case. Regarding Fig. 6(c), the

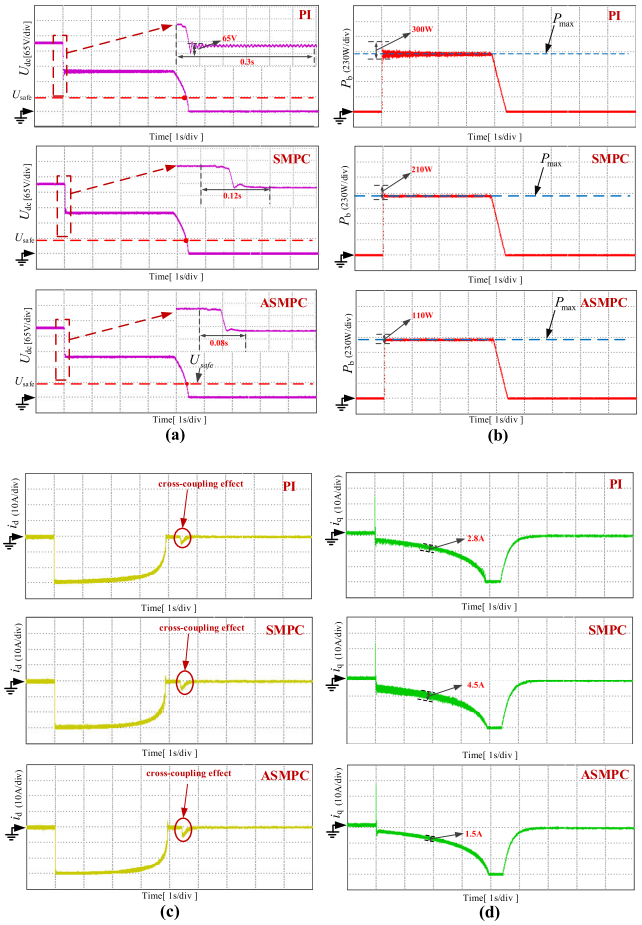

FIGURE 6. Experimental results of the maximum discharge power based on the conventional PI, SMPC and the proposed ASMPC at the speed of 2000 r/min. (a) DC-bus voltage; (b) Discharge power of the external bleeder; (c) d-axis current; (d) q-axis current.

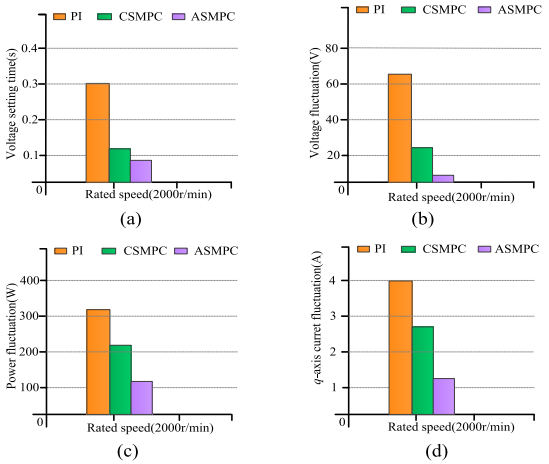

FIGURE 7. Comparison diagram of dynamic performance with three different control methods. (a) Voltage setting time; (b) Voltage fluctuation; (c) Power overshot; (d) q-axis current fluctuation.

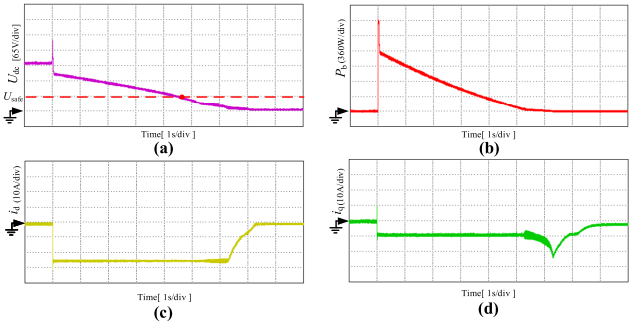

FIGURE 8. Experimental results of the hybrid dc-bus capacitor discharge strategy in [28] at the speed of 2000 r/min. (a) DC-bus voltage; (b) Discharge power of the external bleeder; (c) d-axis current; (d) q-axis current.

d-axis current experiences a sharp decrease when the dc-bus voltage drop to zero. Moreover, the q-axis current begins to increase at the moment. This phenomenon is caused by cross-coupling effect [30], [31]. The dc-bus voltage drops to zero, which means that the d-q axis voltages are all zero at this time. However, there is still energy stored in the motor inductance at this time. Hence, when the dc bus voltage drops to zero, the energy story in the inductance starts to release, which causes the fluctuation of d-axis current. The d-q axis current in Fig.6(c) and (d) has the smallest fluctuation among the three methods, which illustrates that the presented adaptive reaching law can suppress the chattering effectively.

For clarity, Fig. 7 demonstrates the comparison diagram of dynamic performance with three different control methods based on the abovementioned experimental results. From Fig.7, although the CSMPC can improve the dynamic performance, it results in current loop chatting. By contrast, the proposed ASMPC can improve dynamic power performance and suppress the current chatting. It can be seen that the proposed ASMPC is superior in dynamic performance and power fluctuation.

In order to prove the advantage of the proposed discharge method, the hybrid dc-bus capacitor discharge strategy in [28] is conducted and the experimental results is in Fig.8. When the hybrid dc-bus capacitor discharge strategy is implied with the experimental setup, the bleeding resistor value decline to 32Ω (13%) compared with the proposed method. More important, the weight of the BR increases to 5.8 kg (16%). Although the two discharge methods have the same discharge power within 5 seconds, the proposed method reduces the discharge current of the bleeding resistor through maximizing discharge power, thereby reducing the volume and weight of the discharge resistor. Herein, the proposed discharge method can significantly reduce the bleeding resistor weight and size. What 'more, in case of breaking, the proposed discharge method can switch to traditional UR discharge method. Thus, the safety of discharge is ensured.

In order to prove the proposed ASMPC is effective regardless of the machine speed, as demonstrated in Fig.9, the experiment was implemented when the machine speed is 1000r/min. For the sake of low initial speed, the dc-bus capacitor voltage drops to the safe voltage at about 1.25s. Similar to the rated state, the discharge power of the bleeding resistor can track the maximum power as long as the bus voltage is high enough in Fig.9(c). In addition, as the q-axis current decreases until safe current, the d-axis current gradually increases. The q-axis current is gradually

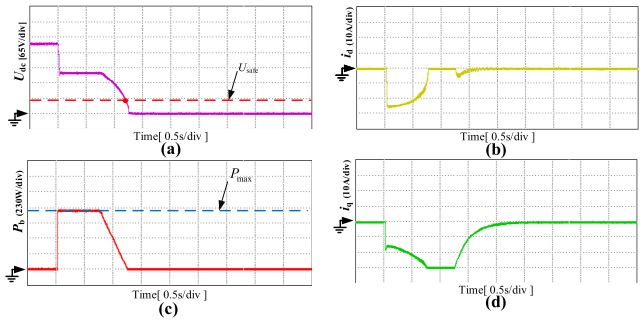

FIGURE 9. Experimental results of the maximum discharge power based on the proposed ASMPC at the speed of 1000 r/min. (a) DC-bus voltage; (b) d-axis current; (c) Discharge power of the external bleeder; (d) q-axis current.

reduced for maintaining the maximum discharge power. The experimental results illustrate that the proposed discharge method can quickly reduce the dc-bus voltage to safe voltage when the EVs encounter an emergency at any speed.

In general, according to the experimental results, the proposed maximum discharge power algorithm based on ASMPC is proven to be able to satisfy the discharge time requirements of United Nation Vehicle Regulation ECE R94 with excellent dynamic performance and small bleeding resistor.

VI. CONCLUSION

This article proposed a novel discharge strategy based on the ASMPC with minimum size and weight of bleeding resistor. Based on the established traditional UR discharge model, the bleeding resistor was designed and evaluated. In order to reduce the size and weight of the bleeding resistor, the maximum discharge power method was proposed based on the power flow model. Compared with the traditional UR discharge method, the volume and weight of the bleeding resistor based on the proposed method was significantly reduced. The ASMPC was proposed to suppress the chattering phenomenon and improve the dynamic performance of the discharge power tracking in the discharge process. By utilizing the adaptive reaching law, the sliding mode chatting and reaching time were reduced conspicuously. The experimental results proved that the proposed method can reduce the discharge bleeder size and weight greatly. Moreover, the ASMPC can obtain an excellent performance with fast response, small overshot and chattering suppression capability. In conclusion, the proposed discharge approach can reduce the dc-bus capacitor voltage to safe voltage in specified time with the designed small bleeding resistor when EVs encounter an emergency, improving the safety of EVs in crash conditions.

REFERENCES

[1] H. Cheng, Z. Wang, S. Yang, J. Huang, and X. Ge, "An integrated SRM powertrain topology for plug-in hybrid electric vehicles with multiple driving and onboard charging capabilities," *IEEE Trans. Transport. Electrific.*, vol. 6, no. 2, pp. 578–591, Jun. 2020.

[2] X. Ding, Z. Wang, L. Zhang, and C. Wang, "Longitudinal vehicle speed estimation for four-wheel-independently-actuated electric vehicles based on multi-sensor fusion," *IEEE Trans. Veh. Technol.*, vol. 69, no. 11, pp. 12797–12806, Nov. 2020.

[3] K. Rajashekara, "Present status and future trends in electric vehicle propulsion technologies," *IEEE J. Emerg. Sel. Topics Power Electron.*, vol. 1, no. 1, pp. 3–10, Mar. 2013.

[4] J. Shen, L. Wang, and J. Zhang, "Integrated scheduling strategy for private electric vehicles and electric taxis," *IEEE Trans. Ind. Informat.*, vol. 17, no. 3, pp. 1637–1647, Mar. 2021.

[5] X. Zhang, J. Yang, and H. Yang, "Robust control of winding-based DC-bus capacitor discharge for PMSM drives in electric vehicles," *IEEE Access*, vol. 9, pp. 123029–123039, 2021.

[6] A. R. Chandran, M. D. Hennen, A. Arkkio, and A. Belahcen, "Safe turn-off strategy for electric drives in automotive applications," *IEEE Trans. Transport. Electrific.*, vol. 8, no. 1, pp. 9–22, Mar. 2022.

[7] C. Gong, Y. Hu, J. Gao, Y. Wang, and L. Yan, "An improved delay-suppressed sliding-mode observer for sensorless vector-controlled PMSM," *IEEE Trans. Ind. Electron.*, vol. 67, no. 7, pp. 5913–5923, Jul. 2020.

[8] G. Bi, G. Wang, G. Zhang, N. Zhao, and D. Xu, "Low-noise initial position detection method for sensorless permanent magnet synchronous motor drives," *IEEE Trans. Power Electron.*, vol. 35, no. 12, pp. 13333–13344, Dec. 2020.

[9] C. Gong, J. Liu, Y. Han, Y. Hu, H. Yu, and R. Zeng, "Safety of electric vehicles in crash conditions: A review of hazards to occupants, regulatory activities, and technical support," *IEEE Trans. Transport. Electrific.*, vol. 8, no. 3, pp. 3870–3883, Sep. 2022, doi: 10.1109/TTE.2021.3136126.

[10] B. Wang, P. Dehghanian, S. Wang, and M. Mitolo, "Electrical safety considerations in large-scale electric vehicle charging stations," *IEEE Trans. Ind. Appl.*, vol. 55, no. 6, pp. 6603–6612, Nov. 2019.

[11] J. I. Itoh, W. Aoki, G. T. Chiang, and A. Toba, "Uniform provisions concerning the approval of vehicles with regard to the protection of the occupants in the event of a frontal collision," United Nation Econ. Commission Eur. Vehicle Regulation, Geneva, Switzerland, Tech. Rep. No.94 (ECE R94), Aug. 2013.

[12] T. Goldammer, T. Le, J. Miller, and J. Wai, "Active high voltage bus bleed down," U.S. Patent 8 610 382 B2, Dec. 17, 2013.

[13] Z. Ke, J. Zhang, and M. W. Degner, "DC bus capacitor discharge of permanent-magnet synchronous machine drive systems for hybrid electric vehicles," *IEEE Trans. Ind. Appl.*, vol. 53, no. 2, pp. 1399–1405, Mar. 2017.

[14] T. Wu, W. Li, Y. Hu, C. Gong, S. Kuka, and J. Lu, "Parameter dependency analysis of uncontrolled generation for IPMSMs in electric vehicles," in *Proc. IECON 45th Annu. Conf. IEEE Ind. Electron. Soc.*, vol. 1, Oct. 2019, pp. 3237–3241.

[15] C. Gong, Y. Hu, G. Chen, H. Wen, Z. Wang, and K. Ni, "A DC-bus capacitor discharge strategy for PMSM drive system with large inertia and small system safe current in EVs," *IEEE Trans. Ind. Informat.*, vol. 15, no. 8, pp. 4709–4718, Aug. 2019.

[16] L. Han, H. Yao, and Y. Xia, "Braking technology and application of VSI bleeder resistor based on maximum power," *Power Electron. Technol.*, vol. 46, no. 8, pp. 83–85, Aug. 2012.

[17] J. W. Meyer III, D. P. Tasky, and S. M. N. Hasan, "Passive high-voltage DC bus discharge circuit for a vehicle," U.S. Patent 9 018 865 B2 Apr. 28, 2015.

[18] M. Hang, W. Lin, and R. Wu, "An active discharge circuit of a motor controller for electric vehicles and its control method," CN Patent 2 012 101 587 108, Oct. 10, 2012.

[19] S. Zhuo, A. Gaillard, L. Xu, D. Paire, and F. Gao, "Extended state observer-based control of DC–DC converters for fuel cell application," *IEEE Trans. Power Electron.*, vol. 35, no. 9, pp. 9923–9932, Sep. 2020.

[20] H. Ríos, R. Falcón, O. A. González, and A. Dzul, "Continuous sliding-mode control strategies for quadrotor robust tracking: Real-time application," *IEEE Trans. Ind. Electron.*, vol. 66, no. 2, pp. 1264–1272, Feb. 2019.

[21] X. Sun, J. Cao, G. Lei, Y. Guo, and J. Zhu, "A robust deadbeat predictive controller with delay compensation based on composite sliding-mode observer for PMSMs," *IEEE Trans. Power Electron.*, vol. 36, no. 9, pp. 10742–10752, Sep. 2021.

[22] Y. Wang, Y. Zhu, X. Zhang, B. Tian, K. Wang, and J. Liang, "Antidisturbance sliding mode-based deadbeat direct torque control for PMSM speed regulation system," *IEEE Trans. Transport. Electrific.*, vol. 7, no. 4, pp. 2705–2714, Dec. 2021.
[23] X. Sun, Y. Xiong, J. Yang, and X. Tian, "Torque ripple reduction for a 12/8 switched reluctance motor based on a novel sliding mode control strategy," *IEEE Trans. Transport. Electrific.*, vol. 9, no. 1, pp. 359–369, Mar. 2023.
[24] T. H. Nguyen, T. T. Nguyen, V. Q. Nguyen, K. M. Le, H. N. Tran, and J. W. Jeon, "An adaptive sliding-mode controller with a modified reduced-order proportional integral observer for speed regulation of a permanent magnet synchronous motor," *IEEE Trans. Ind. Electron.*, vol. 69, no. 7, pp. 7181–7191, Jul. 2022.
[25] X. Zhang and J. Yang, "A robust flywheel energy storage system discharge strategy for wide speed range operation," *IEEE Trans. Ind. Electron.*, vol. 64, no. 10, pp. 7862–7873, Oct. 2017.
[26] G. Feng, C. Lai, X. Tan, and N. C. Kar, "Maximum-torque-per-square-ampere control for interior PMSMs considering cross-saturation inductances," *IEEE Trans. Transport. Electrific.*, vol. 7, no. 3, pp. 1482–1492, Sep. 2021.
[27] H. Yang, J. Yang, and X. Zhang, "DC-bus capacitor maximum power discharge strategy for EV-PMSM drive system with small safe current," *IEEE Access*, vol. 9, pp. 132158–132167, 2021.
[28] C. Gong, Y. Hu, W. Li, J. Gao, J. Liu, H. Wen, and J. Yang, "Hybrid DC-bus capacitor discharge strategy using internal windings and external bleeder for surface-mounted PMSM-based EV powertrains in emergency," *IEEE Trans. Ind. Electron.*, vol. 68, no. 3, pp. 1905–1915, Mar. 2021.
[29] S. Xiaoxia, W. Yichun, M. Lingke, W. Facheng, and X. Longyun, "Research on braking resistor of hybrid electric armored vehicle," in *Proc. Int. Conf. Inf., Netw. Autom. (ICINA)*, vol. 2, Kunming, China, Oct. 2010, pp. V2-206–V2-210.
[30] A. Rabiei, T. Thiringer, M. Alatalo, and E. A. Grunditz, "Improved maximum-torque-per-ampere algorithm accounting for core saturation, cross-coupling effect, and temperature for a PMSM intended for vehicular applications," *IEEE Trans. Transp. Electrific.*, vol. 2, no. 2, pp. 150–159, Jun. 2016.
[31] X. Fang, F. Lin, and Z. Yang, "A modified flux-weakening control method of PMSM based on the d-q current cross-coupling effect," in *Proc. IEEE Conf. Expo. Transp. Electrific. Asia–Pacific (ITEC Asia–Pacific)*, Beijing, China, Aug. 2014, pp. 1–6.

XIAOJUN ZHANG was born in Shandong, China, in 1991. He received the M.Sc. and Ph.D. degrees from Zhejiang University, Hangzhou, China, in 2018 and 2022, respectively.

He is currently a Postdoctoral Research Fellow with Zhejiang University. His research interests include electrical machine drives and power electronics.

JIAQIANG YANG (Senior Member, IEEE) was born in Jiangsu, China, in 1970. He received the Ph.D. degree in electrical engineering from Zhejiang University, Hangzhou, China, in 2004.

Since 2004, he has been a Lecturer, an Associate Professor, and a Professor with the College of Electrical Engineering, Zhejiang University. From 2012 to 2013, he was a Research Fellow with the College of Electrical and Computer, National University of Singapore, Singapore. His research interests include robot vision perception and unmanned driving control, and the design and control of motors for electrical vehicles.